Clim Dyn
DOI 10.1007/s00382-012-1344-x

Tropical precipitation regimes and mechanisms of regime transitions: contrasting two aquaplanet general circulation models

Boutheina Oueslati · Gilles Bellon

Received: 28 June 2011 / Accepted: 15 March 2012

Abstract The atmospheric general circulation models ARPEGE-climate and LMDz are used in an aquaplanet configuration to study the response of a zonally symmetric atmosphere to a range of sea surface temperature (SST) forcing. We impose zonally-symmetric SST distributions that are also symmetric about the equator, with varying off-equatorial SST gradients. In both models, we obtain the characteristic inter-tropical convergence zone (ITCZ) splitting that separates two regimes of equilibrium (in terms of precipitations): one with one ITCZ over the equator for large SST gradients in the tropics, and one with a double ITCZ for small tropical SST gradients. Transition between these regimes is mainly driven by changes in the low-level convergence that are forced by the SST gradients. Model-dependent, dry and moist feedbacks intervene to reinforce or weaken the effect of the SST forcing. In ARPEGE, dry advective processes reinforce the SST forcing, while a competition between sensible heat flux and convective cooling provides a complex feedback on the SST forcing in the LMDz. It is suggested that these feedbacks influence the location of the transition in the parameter range.

Keywords Tropical precipitation regimes · Double ITCZ · Atmospheric dynamics and feedbacks

This paper is a contribution to the special issue on the IPSL and CNRM global climate and earth system models, both developed in France and contributing to the 5th coupled model intercomparison project.

B. Oueslati (✉) · G. Bellon
Centre National de Recherches Météorologiques,
CNRS/Météo-France, 42, Avenue Gaspard Coriolis,
31057 Toulouse Cedex 01, France
e-mail: boutheina.oueslati@meteo.fr

1 Introduction

The intertropical convergence zone (ITCZ) is a prominent feature of the tropical atmosphere that appears as a zonally elongated band of enhanced cloudiness and rainfall, embedded in the upward branch of the Hadley circulation. Observations over the Pacific and Atlantic oceans show that the ITCZ is located around 10°N. This off-equatorial preference location is still poorly understood and it is not well simulated by the general circulation models (GCMs). In fact, most of them produce a double ITCZ with excessive precipitation south of the equator and insufficient precipitation north of the equator. This double structure has been observed over some of the world oceans, particularly over the eastern Pacific during boreal spring (Hubert et al. 1969), but it is too often simulated by GCMs (Dai 2006). This systematic bias of the GCMs is generally referred to as the double ITCZ syndrome (Mechoso et al. 1995) and there is still no consensus on its causes.

Many studies point to the central role of the sea surface temperature (SST) in the control of the ITCZ location. The off-equatorial position of the ITCZ is, in fact, generally associated with the spatial distribution of the SST, particularly the presence of an extended cold tongue on the equator due to the equatorial ocean upwelling. The excessive precipitation, characterizing the double ITCZ problem, affects in turn the SST distribution by increasing the trade winds and producing excessive latent heat flux and insufficient shortwave flux. These all contribute to the significant cold SST bias over much of the tropical oceans (Lin 2007). This SST-precipitation interaction suggests the role played by ocean-atmosphere coupling in the double ITCZ problem, including one or more of the following feedbacks: the SST-wind-induced surface fluxes feedback (Xie and Philander 1994), the SST-stratus feedback

Published online: 03 April 2012

(Philander et al. 1996) involving the shortwave cloud radiative forcing and the SST gradient-trade wind feedback associated with vertical upwelling (Bjerknes 1969). Any excessive positive feedback (or insufficient negative feedback) tends to shift the Walker circulation more westward, leading to an excessive SST cold tongue and, thus, a double ITCZ pattern (Dijkstra and Neelin 1995). Nevertheless, a comparison between GCMs with a double ITCZ pattern indicates that the atmospheric models rather than the ocean models are primaly responsible for this problem (Schneider 2002). Coupled feedbacks tend to amplify the biases of the atmospheric models (Lin 2007; Zhang et al. 2007)

Together with the SST contribution, internal atmospheric mechanisms are proposed to explain the double ITCZ problem, concentrating on the role of near-equatorial dynamics. On the basis of the conditional instability of the second kind (CISK) theory, Charney (1971) proposed that the position of the ITCZ is governed by a balance between moisture convergence associated with efficient Ekman pumping, which increases with the Coriolis parameter, and the boundary layer supply of moisture by surface fluxes, which decreases with SST away from the equator. The combined effect of these two processes determine the ITCZ position, several degrees away from the equator. Other studies explained the latitudinal location of the ITCZ by zonally-propagating waves, particularly the coupling of the wave-CISK modes and transients (Holton et al. 1971; Lindzen 1974; Hess et al. 1993). Both previous theories were discussed in a study by Waliser and Somerville (1994) who argued that convection occurs in the latitude range of about 4°–12° away from the equator, due to the enhanced feedback between the midtropospheric latent heating and the low-level convergence of moist static energy at these latitudes.

These atmospheric mechanisms are model-dependent. We notice, in fact, a large panel of GCMs responses even in simple settings such as aquaplanet configuration. Several studies showed the existence of multiple climate regimes with varying ITCZ structure depending on the imposed solar forcing. Some models exhibit symmetric regimes with single and double ITCZs that are very sensitive to the convection parametrization. Liu et al. (2009) attributed the single ITCZ to a prevailing CISK mechanism at the equator, whereas the double ITCZ was associated with the evaporation–wind feedback. Under the condition of globally and temporally uniform SST and solar insolation angle Chao and Chen (2004), attributed the ITCZ location to a balance between two types of attraction resulting from the Earth's rotation. Some models yield equilibria that are asymmetric with respect to the equator, even under symmetric boundary conditions. Authors point to the role of wind–evaporation-SST feedback and longwave radiative effects of clouds and water vapor (Barsugli et al. 2005) as well as the vertical profile of temperature and the free-tropospheric moisture–convection feedback (Bellon and Sobel 2010) in maintaining these regimes.

All these studies show the complexity of the ITCZ dynamics and the large diversity of GCM responses and feedbacks. To further study the atmospheric internal dynamics of this feature, we analyze, in this paper, the response of two aquaplanet models to various SST latitudinal distributions. The present analysis will, particularly, investigate the existence of multiple regimes, explore their characteristics and untangle the mechanisms at play in regime transition.

The paper is structured as follows. In Sect. 2, we introduce the models and experiment design. In Sect. 3, we present the different regimes of tropical precipitation arising from a range of SST boundary conditions. Section 4 analyzes the transition from the double-ITCZ regime to the single-ITCZ regime. Conclusions are drawn in Sect. 5.

2 Models and experiments design

2.1 The models

We use the version 5.2 of the atmospheric general circulation model (AGCM) ARPEGE-climat (Déqué et al. 1994) and the version 5 of the AGCM LMDz (Hourdin et al. 2006). The two AGCMs are respectively the atmospheric component of the CNRM-CM5 (Voldoire et al. 2011) and the IPSL-CM5A (Dufresne et al., submitted) earth systems used for the coupled model intercomparaison project phase 5 (CMIP5).

ARPEGE is a spectral model that uses a triangular truncation T127, which corresponds to a horizontal resolution of 1.4° at the equator. The model uses an hybrid sigma-pressure vertical coordinate discretized onto 31 vertical levels. The parameterization of radiation combines the longwave radiation scheme rapid radiation transfer model (RRTM, Mlawer et al. 1997) and a shortwave scheme based on the work of Fouquart and Bonnel (1980). The surface fluxes are parameterized using the exchange coefficients from unified multi-campaigns estimates (ECUME) turbulence scheme (Belamari and Pirani 2007). The atmospheric boundary layer is parameterized using a new turbulent kinetic energy scheme (Cuxart et al. 2000). Convection is parameterized by a mass–flux scheme in which triggering depends on atmospheric stability and the closure is a function of moisture convergence (Bougeault 1985). A statistical cloud scheme developed by Ricard and Royer (1993) is included. Energy, water and momentum budgets are diagnosed by the diagnostics over horizontal (DDH domains) tool.

The LMDz is a grid-point model with a horizontal uniform resolution of 3.75° in longitude, 1.9° in latitude, and 39 hybrid vertical levels. The thermal infra-red part of the radiation scheme was introduced by Morcrette et al. (1986). The solar part is an improved version of the Fouquart and Bonnel (1980) scheme. The surface boundary layer is treated according to Louis (1979). Convection is parameterized by the Emanuel (1991)'s mass–flux scheme where closure and triggering take into account both tropospheric instability and convective inhibition. The statistical cloud scheme follows Bony and Emanuel (2001).

2.2 The experiments

For this study, an aquaplanet configuration of these models is used following the CMIP5 recommendations with idealized SST distributions, perpetual equinoctial solar insolation including the diurnal cycle. Aerosols are radiatively inactive and sea-ice formation is neglected in the two models.

The SST distribution is specified in a manner similar to the Aqua–planet experiment project (Neale and Hoskins 2000a). It is zonally symmetric with a maximum set to 27 °C at the equator:

$$\text{if } -\frac{\pi}{3} < \phi < \frac{\pi}{3},$$
$$\mathrm{SST}(\phi) = 27\left(1 - n(1-k)\sin^2\left(\frac{3\phi}{2}\right) - nk\sin^4\left(\frac{3\phi}{2}\right)\right),$$
$$\text{otherwise,} \quad \mathrm{SST}(\phi) = 27(1-n), \tag{1}$$

where ϕ is the latitude; k and n two parameters that control the SST field: n controls the equator-pole SST difference (27° C for $n = 1$ and 0 for $n = 0$); increasing k flattens the SST distribution at the equator, pushing large SST gradients poleward. Figure 1 shows the SST distributions for some values of k and n. Five-year simulations were performed using the final state of a previous aquaplanet simulation as initial conditions. The results are not very different from year to year: the only difference is a small variation in the amplitude of the precipitation maxima. For all the simulations, the first 2 years are not analyzed to avoid spin up effects. The zonal means, averaged over the last 3 years, are analyzed in the following sections. Unless otherwise specified the variables mentioned hereafter are averages in time and longitude.

3 Circulation regimes

With both models, we perform a series of simulations with varying k and n to explore the models response to a range of SST boundary conditions. We obtain various tropical precipitation patterns that we describe by two characteristics: the number of precipitation maxima and the number of moisture convergence zones (i.e., contiguous regions of positive vertically-integrated convergence of humidity). The following water balance of the atmospheric column shows that column-integrated moisture convergence equals the net surface flux:

$$-\int_0^{p_s} \nabla \cdot (q\mathbf{v})\, \frac{\mathrm{d}p}{g} = P - E, \tag{2}$$

where $q\mathbf{v}$ is the horizontal flux of total water, p is the pressure, g is the acceleration of gravity, P is the total precipitation and E is the surface evaporation. The different regimes obtained with ARPEGE and the LMDz are illustrated in Fig. 2 that shows the zonal mean precipitation and moisture convergence for selected simulations. Figure 3 displays the different regimes as function of k and n.

Two precipitation regimes are obtained by both models. The first regime, dubbed "single" regime or "1P" is characterized by one maximum of precipitation confined at the equator. This regime is simulated when the SST distribution peaks at the equator, i.e., for large off-equatorial

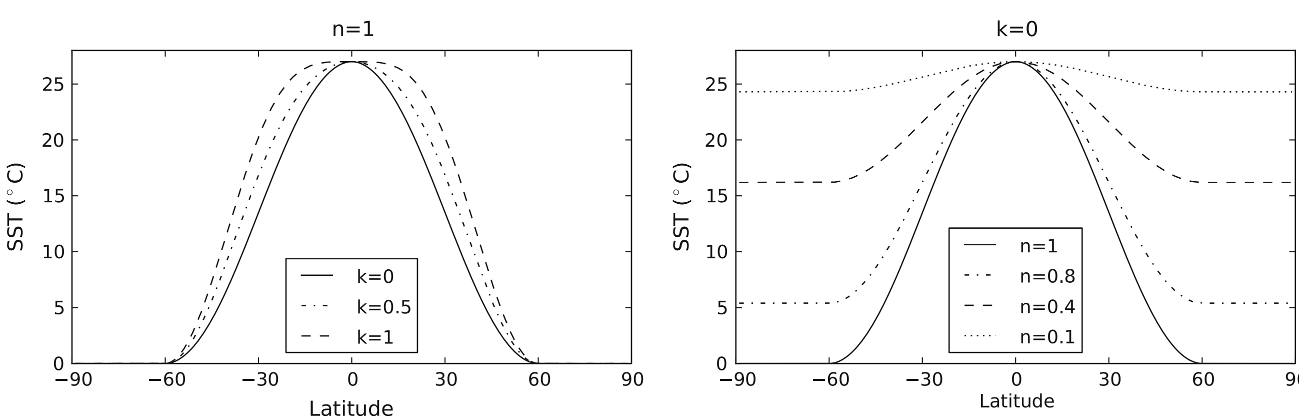

Fig. 1 SST latitudinal distributions for some values of k and n

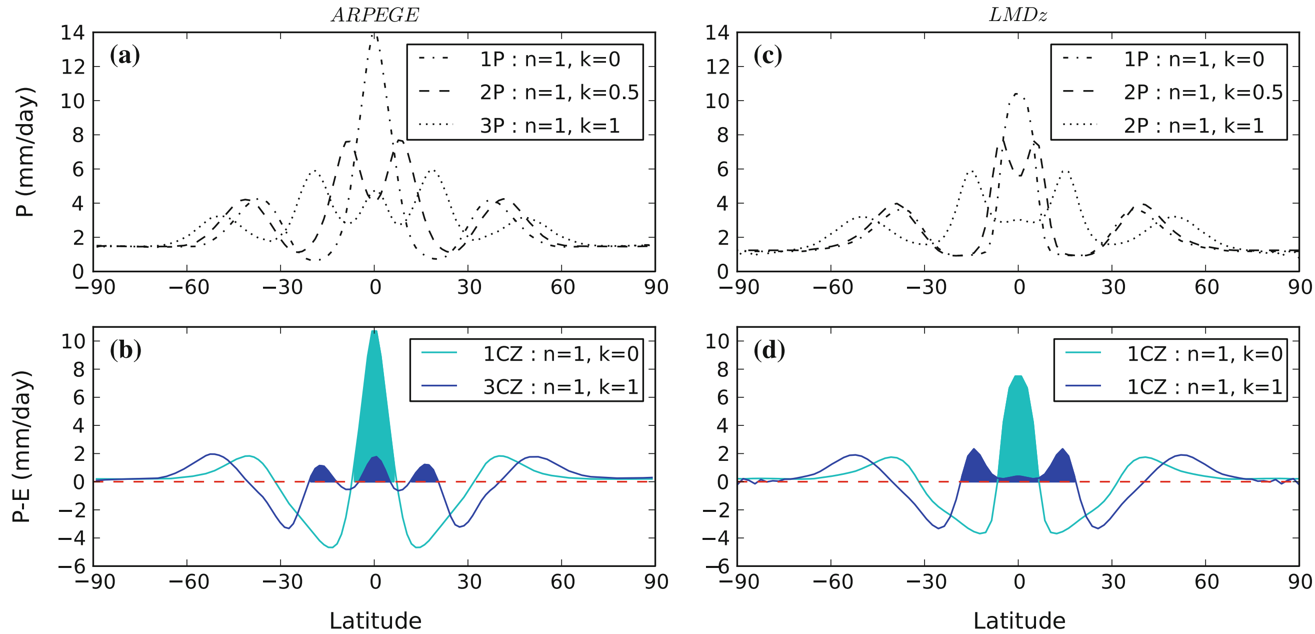

Fig. 2 Stationary zonal-mean precipitation (**a**, **c**) and moisture convergence (**b**, **d**) for various SST forcings. The *shaded areas* correspond to regions of *positive vertically*-integrated convergence of humidity

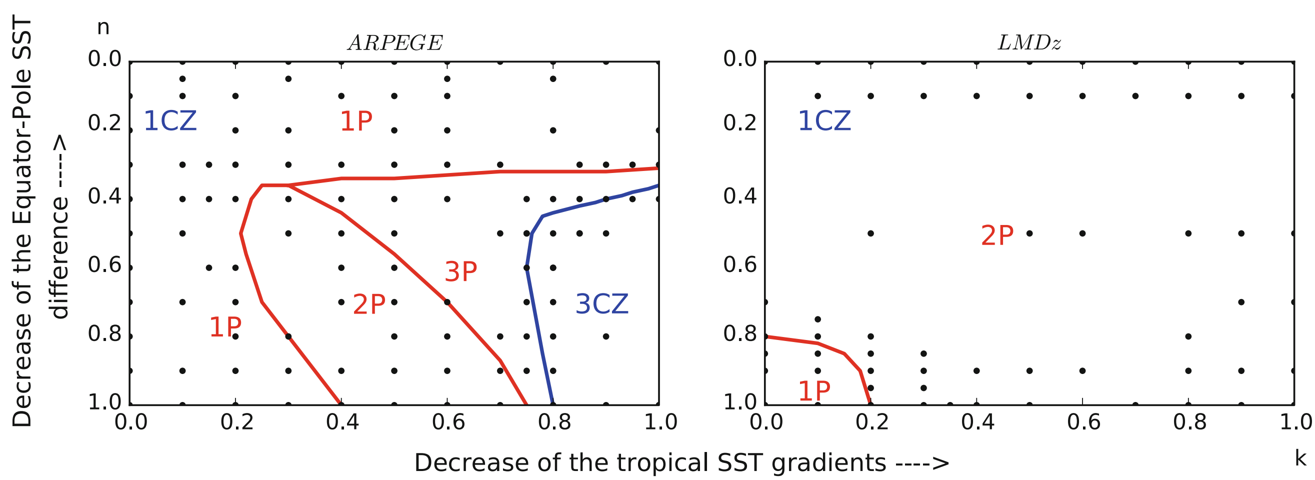

Fig. 3 Circulation regimes simulated by ARPEGE and the LMDz, classified according to the number of maxima of precipitation (*red lines*: 1P, 2P, 3P correspond respectively to 1, 2, 3 maxima) and moisture convergence zones (*blue lines*: 1CZ and 3CZ correspond respectively to 1 and 3 convergence zones). The *dots* indicate the performed simulations

SST gradients. The second regime ("double" regime or "2P") is obtained for weaker tropical SST gradients, in particular for SST distributions similar to the observed one ($n \simeq 1$, $k \simeq 0.5$). It exhibits less intense precipitation at the equator with two off-equatorial peaks (see Fig. 2a, c). For weaker off-equatorial SST gradients, ARPEGE yields a third regime, "3P", with one small precipitation peak at the equator and two off-equatorial, more intense, precipitation peaks. For the same SST distribution, the LMDz simulates only two precipitation maxima at 15°N and S, a finding similar to the results of the HadAM3 AGCM (Neale and Hoskins 2000b). In these models, there is little large-scale vertical motion at the equator and the equatorial atmosphere is close to radiative–convective equilibrium. When the equator–pole SST gradient gets smaller, the 2P regime remains in the LMDz, while ARPEGE transitions from the 2P and 3P regimes to the 1P regime (see Fig. 3). For uniform SST distribution, the two models exhibit an asymmetric, small-amplitude pattern with 4 tropical maxima of precipitation (not shown). This result suggests that a pole to pole uniform SST forcing is sufficient to give rise to an atmospheric general circulation. This spontaneous generation was attributed by previous studies to the earth's rotation and the latitudinal variation of the Coriolis parameter (Chao and

Chen 2004; Kirtman and Schneider 2000). This regime presents an inter-hemispheric symmetry-breaking similar to some of Chao and Chen (2004)'s results.

The precipitation regimes do not coincide with the moisture-convergence regimes. For the range of k and n studied here, we obtained two regimes in ARPEGE: the 1CZ regime with only one convergence zone that is obtained over most of the parameter's range, and one with 3 convergence zones (3CZ) for small tropical SST gradients. The LMDz simulates only the 1CZ regime, although moisture convergence is very small in the regions where the tropical atmosphere is close to radiative-convective equilibrium. For both AGCMs, in the 2P regime (and most of the 3P regime), there is only one ITCZ. None of our simulations yields a double moisture convergence pattern. The double ITCZ syndrom is thus associated hereafter with the 2P precipitation pattern rather than with two moisture convergence zones.

The regimes simulated by AGCMs are clearly model-dependent. We also notice from Fig. 3 that the two models show distinct thresholds for the transition from the double to the single regime. This transition occurs, in the case of ARPEGE, for smaller off-equatorial SST gradients than in the case of the LMDz. This suggests that the LMDz might be more prone to simulate a double ITCZ than ARPEGE. In order to better understand the mechanisms that control the 2P → 1P transition threshold, we further examine this transition in both models in the next section.

4 Mechanisms of the transition from double to single inter-tropical convergence zone (ITCZ)

4.1 Time-dependent behavior of the 1P ↔ 2P transition

To study the 1P ↔ 2P transition, we performed two sets of experiments for 2 months. The first corresponds to the 1P regime setting (with $n = 1$, $k = 0$) but with a 2P initial state (with $n = 1$, $k = 0.5$), to study the 2P → 1P transition. The second corresponds to the 2P regime setting but with a 1P initial state, to study the 1P → 2P transition. We explore the evolution of the 1P ↔ 2P transition from the beginning of each experiment by plotting time-latitude diagrams (see Fig. 4) of precipitation, evaporation and column-integrated moisture convergence defined by the following equation:

$$-\int_0^{p_s} \nabla \cdot (q\mathbf{v}) \frac{\mathrm{d}p}{g} = \frac{[\partial W]}{\partial t} + P - E, \qquad (3)$$

where W is the column-integrated total water.

In Fig. 4, we show ARPEGE results. LMDz yields similar patterns. The precipitation pattern in the 2P → 1P transition (see Fig. 4a) shows a double ITCZ structure in the first day of the experiment that merges into a single ITCZ at around day 15. The reverse transition (see Fig. 4b) is slower and the precipitation pattern shifts from a single to a double ITCZ after day 30. We notice that moisture convergence is driving both transitions (see Fig. 4e, f) and that evaporation is not a crucial element in the 1P ↔ 2P transition (see Fig. 4c, d). The contribution of the different processes at play in the transient behavior of the models are very similar to their contribution to the difference between regimes; hence, we document the mechanisms that explain the difference between the stationary states 1P and 2P in the next section rather than documenting the time evolution of the transition 2P → 1P or 1P → 2P.

4.2 Changes in low-level circulation drive the transition

Here, we investigate the mechanisms responsible for the 2P → 1P transition from the double regime to the single regime by examining the differences between a simulation 1P and a simulation 2P. This transition is forced by the change in SST latitudinal distribution, and we focus on the mechanisms and feedbacks that mediate this forcing in the atmosphere. The change in precipitation results from changes in evaporation and in column-integrated moisture convergence. Their relative contributions over the tropics are shown in Fig. 5. The two models have comparable behaviors, although larger precipitation and evaporation are observed in ARPEGE. We notice that the impact of moisture convergence largely exceeds that of surface evaporation. The 2P → 1P transition is therefore driven by changes in moisture convergence. The difference in evaporation actually favors precipitation away from the equator and constitutes a negative feedback on the 2P → 1P transition. It results mostly from the wind–evaporation effect associated with the equatorward shift of trade winds that accompanies the transition (not shown).

Figure 6 shows the difference in horizontal moisture convergence associated to the 2P → 1P transition. The two models exhibit the very similar moisture convergence patterns and we only show the results from ARPEGE. Changes are confined in the atmospheric boundary layer (ABL) between 800 and 1000 hPa, because the boundary layer is far moister than the free troposphere. There, moisture convergence in 1P is larger between 5°S and 5°N than in 2P, and smaller between 5° and 15° in both hemispheres. The difference in moisture convergence can be decomposed into 5 terms:

$$\Delta(-\nabla \cdot (q\mathbf{v})) = -\bar{q}\,\nabla \cdot \mathbf{\Delta v} - \Delta q\,\nabla \cdot \bar{\mathbf{v}} - \mathbf{\Delta v} \cdot \nabla \bar{q} - \bar{\mathbf{v}} \cdot \nabla \Delta q + \Delta \mathrm{Res}_q, \qquad (4)$$

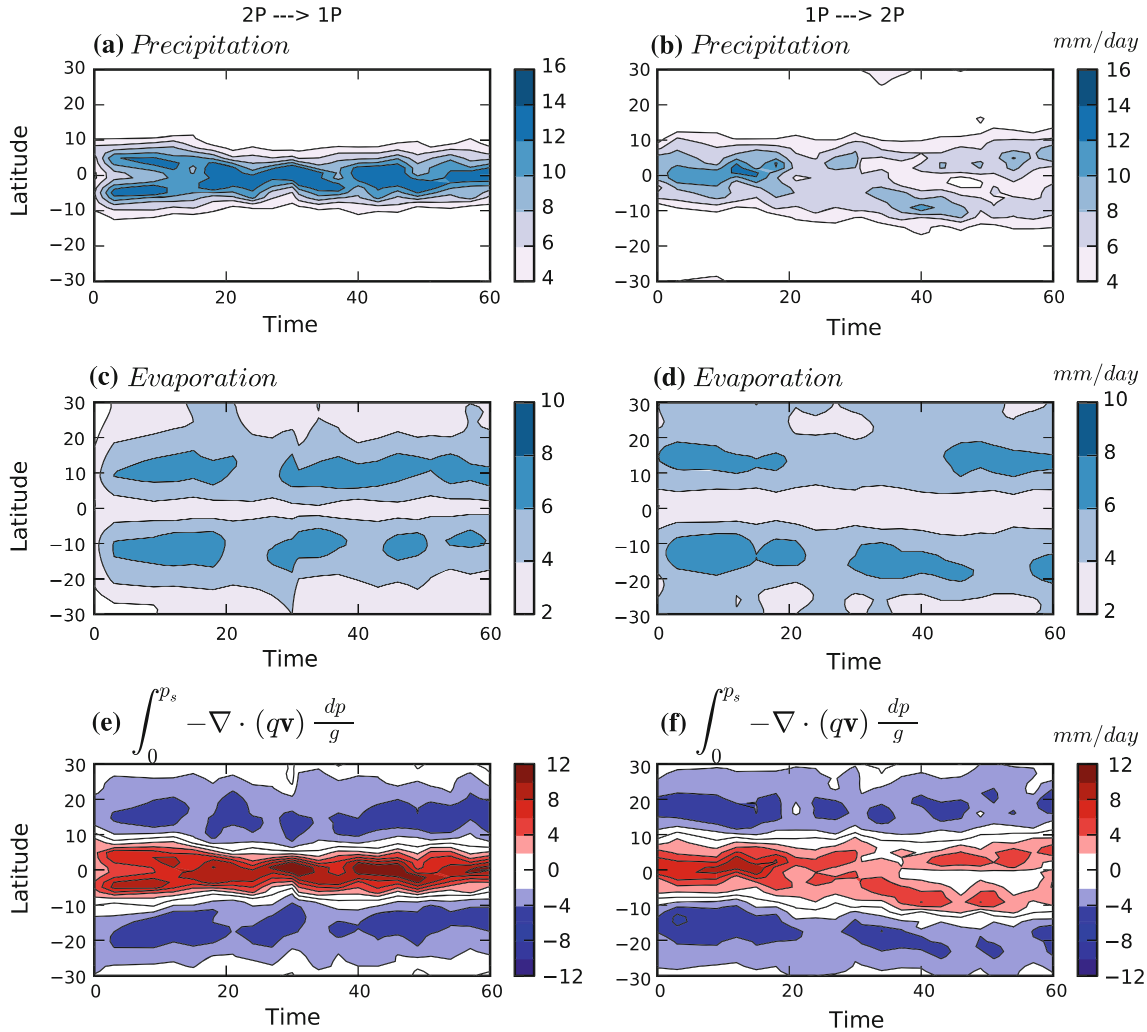

Fig. 4 Time-latitude section of precipitation, evaporation and column-integrated moisture convergence (**a**, **c**, **e** for the 2P → 1P transition; **b**, **d**, **f** for the 1P → 2P)

where q is the total water ratio and $\mathbf{v}$ is the horizontal velocity. The overbar indicates the average between the simulations 1P and 2P, and Δ indicates the difference between these two simulations. Res_q is the residual of the decomposition and combines both zonally-asymmetric patterns and moisture transport due to transient eddies. The first term on the right hand side (rhs) of Eq. (4) is associated with the difference in convergence of the horizontal wind; the second term is associated with the change in humidity of the converging air; the third term is associated with the change in the intensity of horizontal winds, and the fourth with the change in moisture gradients.

Note that, since the variables are zonal averages, only the meridional component is non-zero in the advections and divergences:

$$\mathbf{v}\cdot\nabla = \frac{1}{r}\,v\,\partial_\phi \quad \text{and} \quad \nabla\cdot\mathbf{v} = \frac{1}{r\cos\phi}\,\partial_\phi v,$$

where v is the meridional wind and r is the earth radius. Figure 7 shows these different contributions to the moisture convergence changes for ARPEGE. The results from the LMDz yields similar patterns.

We notice that difference in moisture convergence is driven by changes in low-level flow, mostly through changes in the convergence of the horizontal wind. The change in the humidity field yields contributions that are one order of magnitude smaller than the change in wind convergence. The 2P → 1P transition is thus mediated by the ABL dynamics, which controls the low-level moisture convergence. An analysis of the ABL momentum budget (not shown) confirms that the low-level wind results from a quasi-linear balance between horizontal geopotential gradient, surface friction and Coriolis acceleration as expected from classical theories (e.g., Lindzen and Nigam 1987). The next paragraph focuses on the processes that control the ABL geopotential gradients and, therefore, the low level circulation.

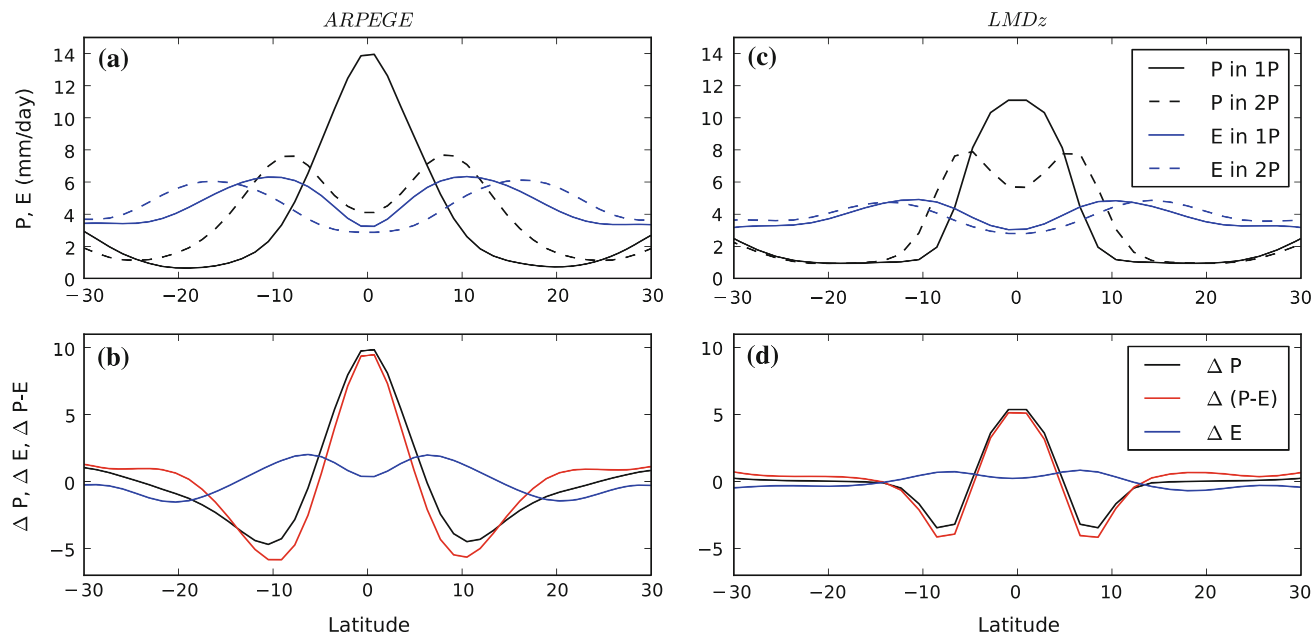

Fig. 5 **a**, **c** Zonal-mean precipitation and evaporation for the regimes 1P and 2P. **b**, **d** Difference in zonal-mean evaporation ΔE, zonal-mean precipitation ΔP and vertically-integrated moisture convergence $\Delta(P - E)$ between the single and double regimes

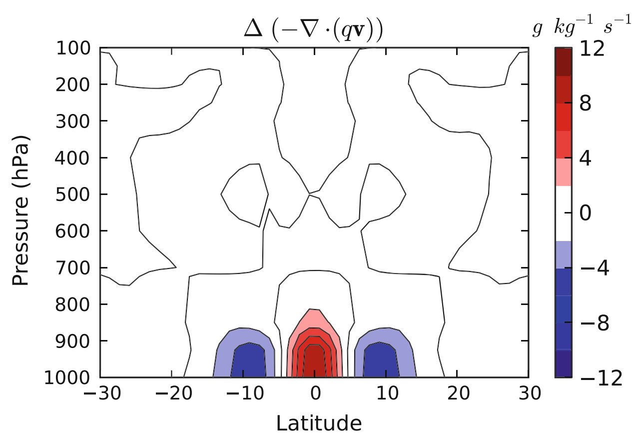

Fig. 6 Difference in the zonal-mean convergence of the *horizontal* moisture flux between the *single* and *double* regimes

4.3 Boundary layer temperature gradients versus upper-level forcing

By integrating the hydrostatic equation, ABL geopotential gradient can be expressed as the sum of the ABL-top geopotential gradient and the vertical integral of the ABL temperature:

$$\Delta\,\nabla\Phi_{(p)} = \Delta\,\nabla\Phi_{(800\,\mathrm{hPa})} - \int_{800}^{p} R\,\nabla\Delta T\,\frac{\mathrm{dp}}{p} \qquad (5)$$

where Φ is the geopotential, T the temperature and R the specific gas constant (287 J kg^{-1} K^{-1}). As previoulsly, Δ indicates the difference between the simulations 1P and 2P.

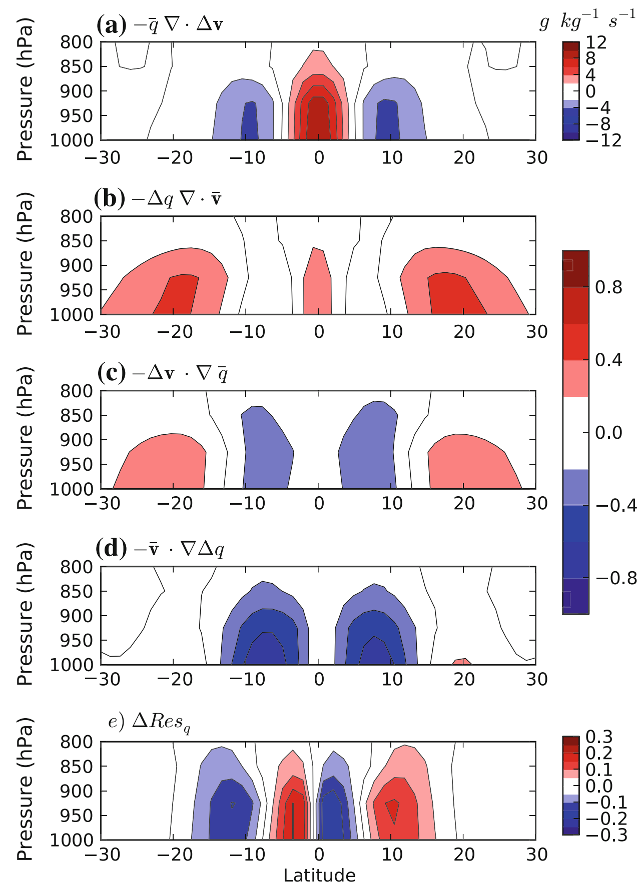

Fig. 7 Zonal-mean contributions to the horizontal moisture convergence changes. **a** $-\bar{q}\nabla\cdot\Delta\mathbf{v}$, **b** $-\Delta q\nabla\cdot\bar{\mathbf{v}}$, **c** $-\Delta\mathbf{v}\cdot\nabla\bar{q}$, **d** $-\bar{\mathbf{v}}\cdot\nabla\Delta q$, and **e** the residual of the decomposition $\Delta\mathrm{Res}_q$

The second term on the rhs of Eq. (5) will be hereafter noted $\Delta\nabla\Phi_{ABLT}$.

The geopotential gradient is negligible at the top of the atmosphere (see $\Delta\nabla\Phi_{(10hPa)}$ in Fig. 9, 10 hPa corresponding to the highest model pressure level). This is expected to result from the overall diffusive effect of the upper-atmosphere wave dynamics. Considering this property, the 800-hPa geopotential gradient results, through the hydrostatic equation, from the free-tropospheric and stratospheric temperature gradients that are controlled by tropospheric convective heating and stratospheric cooling. The first process is at the heart of the Gill model (Gill 1980) which is based on the assumption that the low-level convergence is generated by the mid-tropospheric latent heating. The stratospheric cooling associated with the tropospheric latent heating, generally termed "cold top", has been documented in observations and reanalyses. Holloway and Neelin (2007) presented a brief review of the relevant literature and proposed one common mechanism explaining the cold top. They showed that the cooling results from broad adiabatic ascent forced by convection. The cold top is thought of as a necessary response to convective heating in order to reduce the anomalous geopotential gradients in the upper layers of the atmosphere. The second contribution to the low-level convergence results from ABL temperature (ABLT) gradients that are expected to result from SST gradients through turbulent processes as suggested by Lindzen and Nigam (1987).

Figure 8 shows the difference in temperature between the simulations 1P and 2P. In the upper-troposphere and stratosphere, this change in temperature is strongly model-dependent. In ARPEGE, convection in the 1P regime is more intense than in the 2P regime. The convective heating reaches, therefore, higher altitudes in the 1P regime than in the 2P regime, explaining the positive anomaly of temperature observed in ARPEGE around 200 hPa. The cold top is also cooler in the 1P regime than in the 2P regime, because of the more intense convection. The LMDz has a similar behavior, but with a much smaller amplitude. The inter-model differences in the parameterization of moist convection are a leading explanation for the difference in the convection magnitude between the two models. In Emanuel's scheme the closure is a function of the tropospheric stability. By warming the upper layers, convection moderates itself in the LMDz (see Fig. 2c). In Bougeault's scheme, the moisture convergence closure does not provide a strong sensitivity to the atmospheric stability, allowing large rain rates such as those obtained in the ARPEGE's 1P regime (see Fig. 2a). In the mid-troposphere and ABL, the two models simulate similar temperature differences between the simulations 1P and 2P. In the ABL, changes in temperature are fairly barotropic, so the changes in geopotential associated to the change in ABL temperature (ABLT) are expected to follow the same horizontal pattern throughout the ABL. We hereafter focus on the 1000 hPa level to illustrate the different contributions to the change in geopotential gradient. Figure 9 shows the contribution from the stratosphere and free troposphere $(\Delta\nabla\Phi_{(800\,hPa)})$ and the contribution from the ABL $(\Delta\nabla\Phi_{ABLT})$ to the difference in 1000-hPa geopotential gradient.

In ARPEGE, $\Delta\nabla\Phi_{(800\,hPa)}$ is small between 10°S and 10°N. There, the 1000-hPa geopotential gradient is controlled by the ABLT gradient. The diabatic heating and cold top play no direct role near the equator in the surface convergence pattern and are better regarded as consequences rather than causes of the boundary layer convergence, as suggested in previous studies (Back and Bretherthon 2008). In the LMDz, the ABL geopotential gradient is also driven by ABLT gradients. This

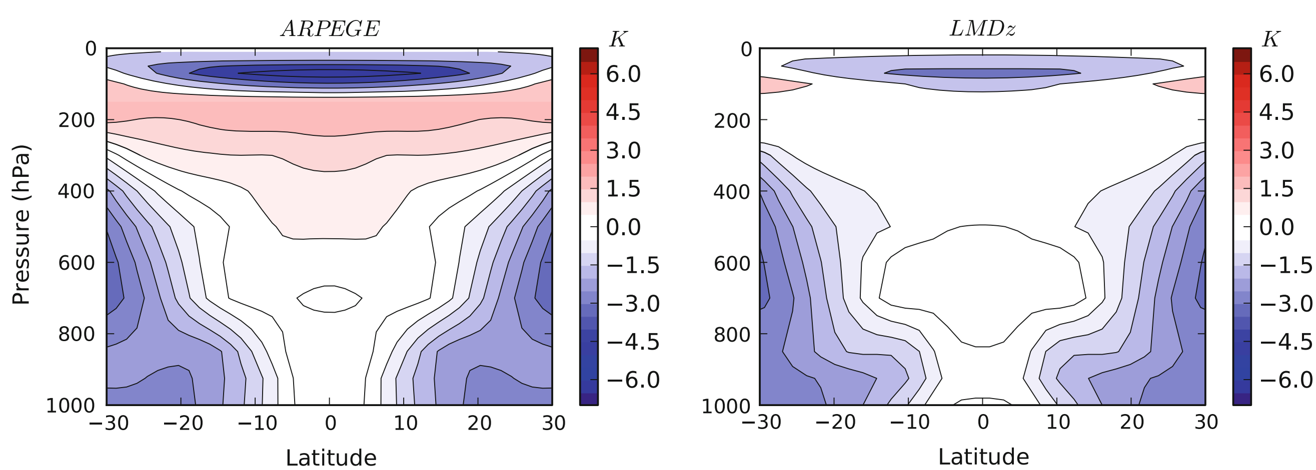

Fig. 8 Difference in temperature between the single and double regimes. Contour intervals are 0.5 K up to 200 hPa and 1.5 K above

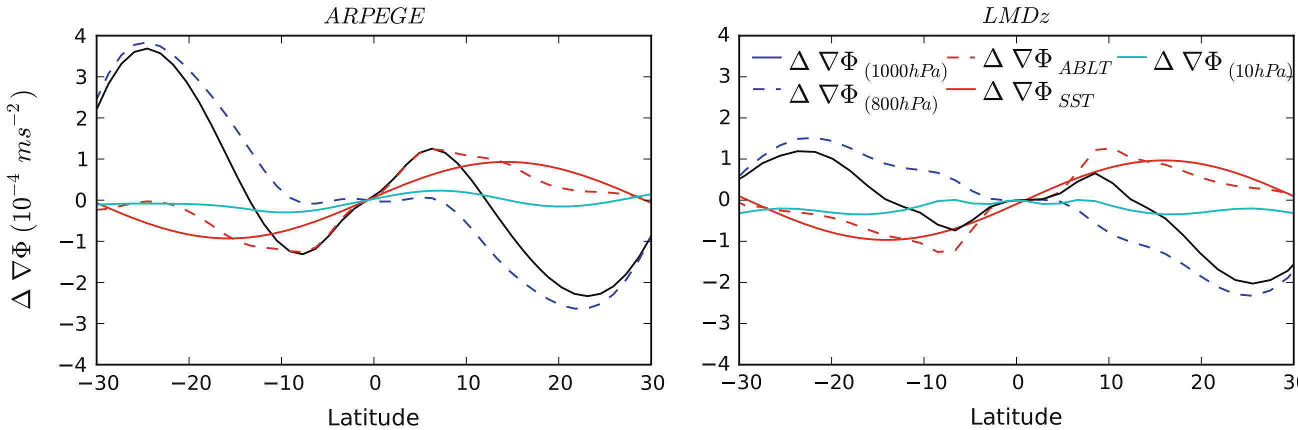

Fig. 9 Difference between the single and double regimes in the zonal mean 1000 hPa geopotential gradient $\Delta\nabla\Phi_{(1000\,\mathrm{hPa})}$, 800 hPa geopotential gradients ($\Delta\nabla\Phi_{(800\,\mathrm{hPa})}$), 10 hPa geopotential gradients ($\Delta\nabla\Phi_{(10\,hPa)}$), vertical integral of the ABLT gradient $\Delta\nabla\Phi_{\mathrm{ABLT}} = -\int_{800}^{1000} R\,\nabla\Delta T\,\frac{\mathrm{d}p}{p}$ and vertical integral of the SST gradient $\Delta\nabla\Phi_{\mathrm{SST}} = -\int_{800}^{1000} R\,\nabla\Delta\mathrm{SST}\,\frac{\mathrm{d}p}{p}$

contribution is, however, weakened by the contribution from the upper layers that combines both the free-tropospheric latent heating and associated cold top. Surprisingly, in this model, the 800-hPa geopotential gradient is driven by the temperature gradients associated with the cold top rather than by those associated with the convective heating (see Fig. 8). Deep convection acts, through the associated cold top, as a negative feedback on the low-level convergence. We also notice that $\Delta\,\partial_\phi\Phi_{\mathrm{ABLT}}$ is weaker around the equator in the LMDz than in ARPEGE. In the subtropical region (15–30°), the difference in stratospheric temperature gradients between the simulations 1P and 2P becomes the main contribution to the difference in 1000-hPa geopotential gradient, for both AGCMs.

The ABLT is expected to be tied to the SST by the turbulent sensible heat flux. Figure 9 also shows the change in geopotential gradient $\Delta\,\partial_\phi\Phi_{\mathrm{SST}}$ that would occur if the ABLT change equalled the underlying SST change. It shows that the difference in ABLT gradients between ARPEGE simulations 1P and 2P is larger than the change in SST gradients between 15°S and 15°N. In the LMDz, the ABLT difference between simulations 1P and 2P is smaller than the SST difference around the equator. As a result, $\Delta\nabla\Phi_{\mathrm{ABLT}}$ is smaller (in magnitude) than $\Delta\,\partial_\phi\Phi_{\mathrm{SST}}$ between 5°S and 5°N and larger between 5° and 12° in both hemispheres. The next section analyzes the reasons for the magnitude of this ABLT response.

4.4 ABL temperature (ABLT) changes

In order to isolate the mechanisms responsible for ABLT changes in the equatorial band, we consider the difference between the temperature budgets across the 2P → 1P transition:

$$\Delta\frac{\partial T}{\partial t} = 0 = \Delta Q_{\mathrm{adv}} + \Delta Q_{\mathrm{conv}} + \Delta Q_{\mathrm{LSC}} + \Delta Q_{\mathrm{rad}} + \Delta Q_{\mathrm{ABL}}, \tag{6}$$

where ΔQ_{adv} is the difference in total advective tendency (advection of temperature and conversion of potential energy) between the simulations 1P and 2P, ΔQ_{conv} is the contribution of convection, ΔQ_{LSC} is the contribution of large-scale condensation (and evaporation), ΔQ_{rad} is the radiative contribution, and ΔQ_{ABL} is the contribution from turbulence and vertical diffusion.

These differences in the temperature tendencies at 1000 hPa are shown for both models in Fig. 10 and are analyzed in the following paragraphs.

4.4.1 *ARPEGE: dynamical control of ABL temperature (ABLT)*

In ARPEGE, ΔQ_{adv} drives the increase of equatorward temperature gradients between 10°S and 10°N. Advection is the main process reponsible for the enhanced change in ABLT gradients compared to the change in SST gradients. The radiative contribution ΔQ_{rad} constitutes another, moderate positive feedback, while the contributions from the large-scale condensation ΔQ_{LSC} and from the surface sensible heat flux ΔQ_{ABL} are negative feedbacks.

The dynamical contribution ΔQ_{adv} is mainly driven by the horizontal component of advection. The vertical component is very small because the vertical wind velocity ω is very small near the surface. Horizontal advection tends to cool the off-equatorial ABL due to the advection of cold subtropical air. An increase of this advection, therefore, contributes to the increase of ABLT gradients between the equator and the off-equatorial regions. The difference in

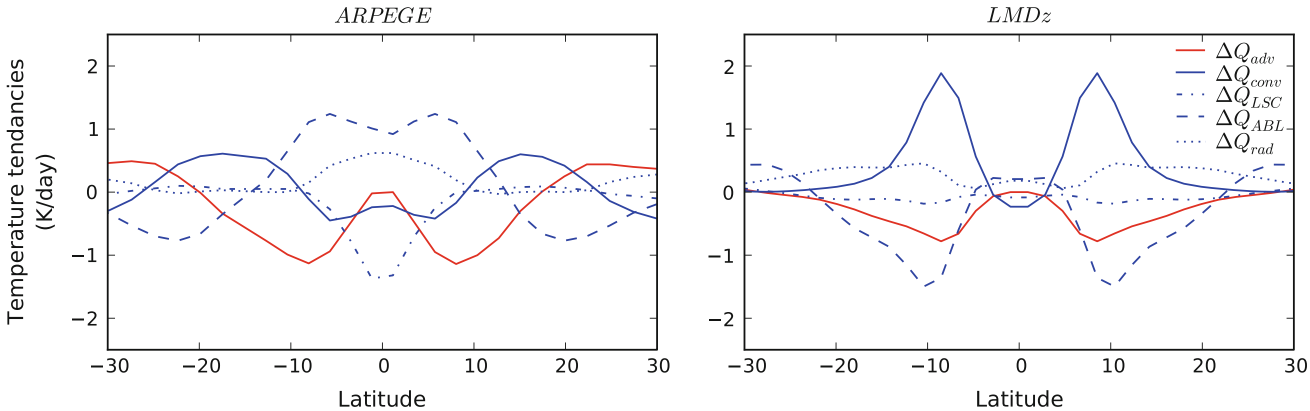

Fig. 10 Difference between the *single* and *double* regimes in the zonal-mean temperature tendencies due to dynamical and physical processes at 1000 hPa

horizontal advection can be associated with the change in horizontal wind and the change in temperature gradient as follows:

$$\Delta(-\mathbf{v}\cdot\nabla T) = -\Delta\mathbf{v}\cdot\nabla\overline{T} - \overline{\mathbf{v}}\cdot\nabla\Delta T + \Delta\mathrm{Res}_T, \qquad (7)$$

where Res_T is the residual of the decomposition and combines both zonally-asymmetric patterns and horizontal advection by the eddies. The different terms of Eq. (7) are shown in Fig. 11 for ARPEGE. Both larger meridional winds and larger ABLT gradients increase the off-equatorial cooling, with a larger contribution from the change in ABLT gradient. The eddies, on the other hand, reduce the off-equatorial cooling.

The change in radiative cooling ΔQ_{rad} is driven by the longwave contribution. The intense equatorial convection in simulation 1P moistens the equatorial troposphere and increases the equatorial cloudiness, resulting in a larger greenhouse effect than in the simulation 2P and favoring off-equatorial ABLT gradients. On the other hand, the contribution of large scale condensation ΔQ_{LSC} is the main negative feedback to the changes in temperature gradients; its change across the 2P $\rightarrow$ 1P transition cools

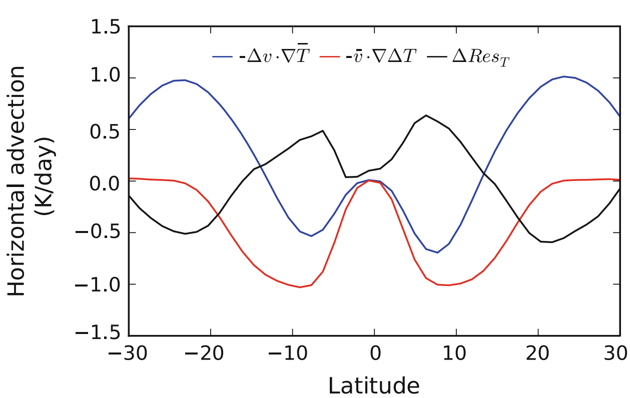

Fig. 11 Zonal-mean contributions to the change in *horizontal* advection of temperature

the equatorial ABL due to the re-evaporation of falling precipitation, reducing the equatorward temperature gradients. The change in convective heating ΔQ_{conv} is fairly uniform in the equatorial band; it warms the subtropical ABL, promoting smaller temperature gradients in the subtropics.

The change in the turbulent contribution ΔQ_{ABL} is due to the change of surface sensible heat flux. This change in surface flux combines contributions from the change in SST-surface air temperature difference and from surface-wind changes, both of which increase off-equatorial surface fluxes. The resulting contribution constitutes a small negative feedback on the change in ABLT gradients.

4.4.2 *LMDz: competition between sensible heat flux and convective cooling*

In the LMDz, the main changes in the ABLT budget are the compensating contributions of turbulence ΔQ_{ABL} and the convection ΔQ_{conv} (see Fig. 10). The former favors off-equatorial ABLT gradients while the latter tends to reduce them. The advective contribution ΔQ_{adv} reinforces the effect of turbulence. The other contributions (ΔQ_{rad} and ΔQ_{LSC}) are fairly uniform accross the tropics, and therefore have little effect on the ABLT gradients. The competition between the main contributions explains the complex pattern of ABLT gradients in the tropics. According to the resulting gradients in Fig. 9, the effect of ΔQ_{conv} dominates between 5°S and 5°N, where the change in ABLT gradients is smaller than the change in SST gradients, and the effect of $\Delta Q_{\mathrm{ABL}} + \Delta Q_{\mathrm{adv}}$ dominates between 5° and 12°.

The change in convective heating ΔQ_{conv} results from a change in the downdrafts (not shown). The convection around 10° is much weaker in the 1P simulation than in the 2P simulation (see Fig. 5c); as a result, the ABL downdraft cooling at these latitudes is much smaller in the 1P simulation than in the 2P simulation. This reduces the off-equatorial ABLT gradients.

The change in surface sensible heat flux, that explains the turbulent contribution ΔQ_{ABL}, results from the competition of the effect of surface wind versus the effect of the air-sea temperature difference. The former opposes off-equatorial ABLT gradients while the latter promotes them (not shown). But the surface-wind effect is small in the LMDz (as can be seen from the evaporation pattern in Fig. 5d), and the air-sea temperature difference is dominant. Furthermore, in the LMDz, the tendencies due to the different physical parameterizations are incremented sequentially, so that the turbulent tendencies are computed on the basis of variables in which the convective contribution is already included. As a result, the air-sea temperature difference used to compute ΔQ_{ABL} takes into account the convective contribution ΔQ_{conv}. This explains why the pattern of ΔQ_{ABL} is similar to that of ΔQ_{conv}, although with opposite sign.

The advective contribution ΔQ_{adv} follows the same pattern as in ARPEGE, but with a smaller magnitude, due to smaller changes in both ABLT gradients and wind.

4.4.3 *Model-dependent behaviors*

In summary, ARPEGE produces a strong, positive, dry, dynamical feedback on the change in SST that favors the transition from the 2P to the 1P regime. This feedback involves the enhancement of off-equatorial ABLT gradients by horizontal advection, that increase the off-equatorial ABL geopotential gradients which, in turn, increase the equatorial convergence. On the other hand, the LMDz produces two negative feedbacks on the same transition, both associated with moist convection: one is due to the stratospheric temperature gradients associated with the cold top, that tend to reduce the off-equatorial geopotential gradients throughout the troposphere all the way down to the ABL. The second feedback is due to the cooling effect of downdrafts that tend to cool the ABL away from equator in the 2P regime and not in the 1P regime and therefore, reduces the change in off-equatorial ABLT gradients accross the 2P $\rightarrow$ 1P transition. As a result, the LMDz precipitation pattern is less sensitive to the latitudinal SST distribution than in ARPEGE (as can already be seen in Fig. 2), and the transition 1P $\leftrightarrow$ 2P is smoother (i.e., occurs over a wider range of k) for LMDz than for ARPEGE. The different feedbacks at play in this regime transition for both models are summarized in Fig. 12.

For $n = 1$ and k between 0.45 and 0.5, where the latitudinal distribution of SST is similar to the observed SST longitudinaly averaged over the oceans, the LMDz and ARPEGE simulate similar 2P precipitation patterns. From this value of k, the parameter k has to be reduced significantly more in order to reach the transition 2P $\rightarrow$ 1P for the LMDz (down to $k \approx 0.2$) than for ARPEGE (down to $k \approx 0.45$) because of the different feedbacks at play in the two models. However, this dominance of the 2P regime in most of the parameter range in LMDz does not indicate an inferior performance of LMDz. It only indicates that, in axisymmetric settings, LMDz is more likely to produce a double ITCZ. This could be seen from April atmosphere-only simulations (i.e., atmospheric model intercomparaison project (AMIP) type) with CNRM-CM5 and IPSL-CM5A models over eastern Pacific (see Fig. 13 left). In this region at this time of the year, a second ITCZ is regularly observed South of the equator. In these fairly axisymmetric and oceanic conditions, which approximate the aquaplanet settings, LMDz shows a more pronounced double ITCZ compared to ARPEGE, but with more intense precipitation than observed. On the other hand, ARPEGE does produce a large amount of precipitation south of the equator in the Central Pacific in July (see Fig. 13 right), because it simulates too zonally-elongated south Pacific convergence zone (SPCZ), while the LMDz represents better this convergence zone. We believe that this bias results in large part from longitude-dependent interaction between the west-Pacific warm pool, the equatorial cold tongue, and the localized intrusion of subtropical eddies, all of which are absent in the axisymmetric framework.

The model behaviors are wildly different from each other. The main reason for this is most plausibly the absence of downdrafts in ARPEGE's parameterization of convection. To some extent, the large-scale re-evaporation of precipitation, in conjunction with the convective heating, plays a role in ARPEGE similar to the role of convective heating, driven by downdraft cooling, in the LMDz (see Fig. 10). But the pattern of $\Delta Q_{\mathrm{conv}} + \Delta Q_{\mathrm{LSC}}$ is much smoother in ARPEGE than its counterpart in the LMDz. Another reason is the difference in the heating profile associated with the parameterized convection. In ARPEGE, the stratospheric cold top and tropospheric heating combine to neutralize their contribution to the ABL geopotential gradients, while in the LMDz the effect of the cold top is still felt at low level.

Some other aspects might play a role in the differences between models. The influence of surface-flux parameterization on the tropical precipitation pattern has already been emphasized by previous studies (e.g., Numaguti 1993); the numerical implementation of the time integration in LMDz might have an influence on the precipitation pattern by computing the surface fluxes using the convectively-adjusted atmospheric variables.

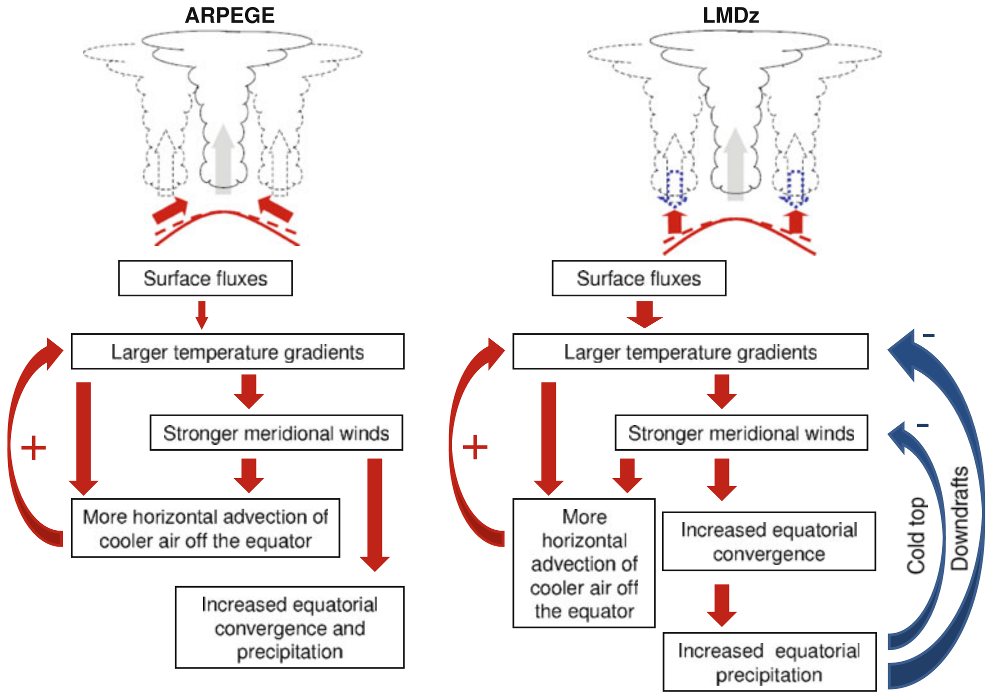

Fig. 12 Schematic of the atmospheric feedbacks at play in the transition from the 2P to the 1P regime in ARPEGE and LMDz. *Red arrows* refer to *positive* feedbacks. *Blue arrows* refer to *negative* feedbacks

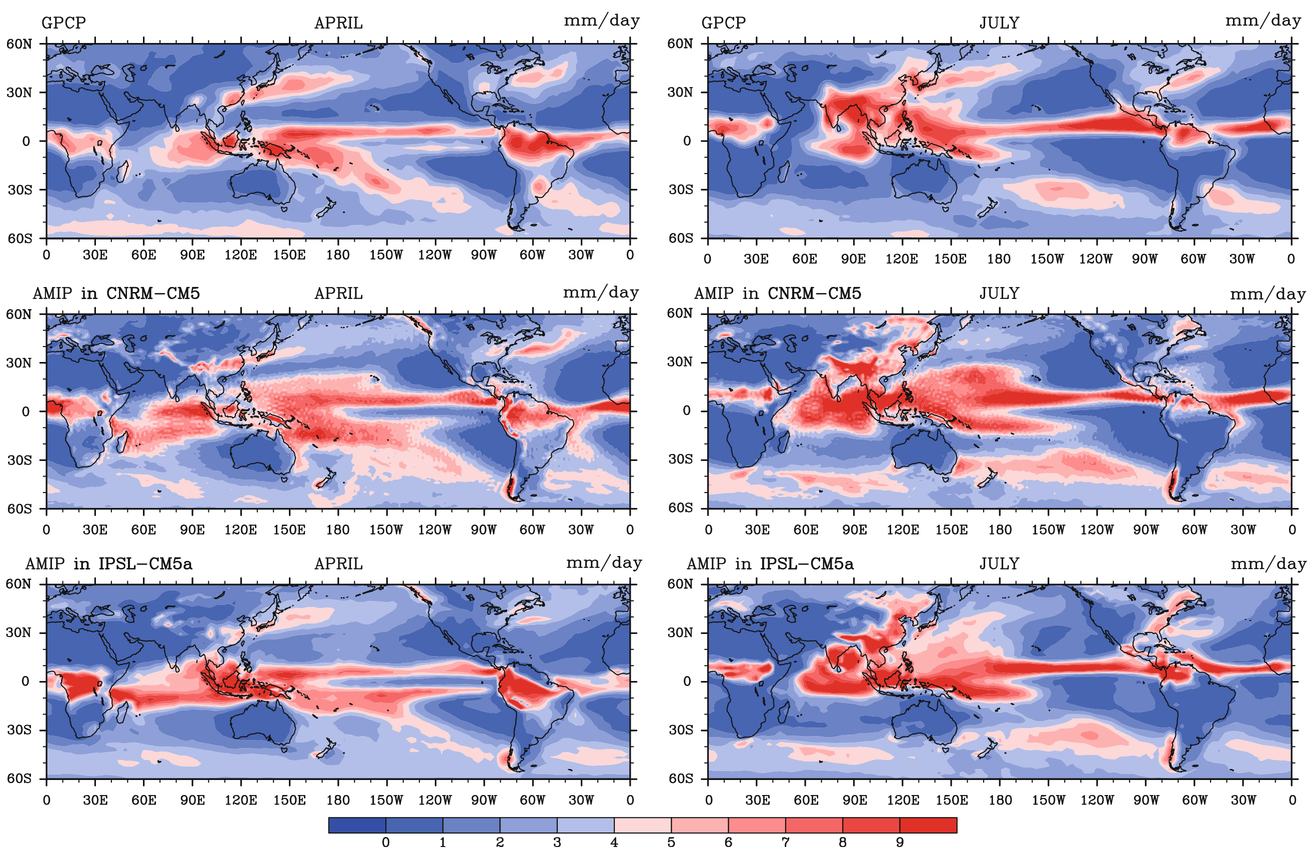

Fig. 13 1979–2001 mean precipitation from GPCP data, AMIP configuration of CNRM-CM5 model (ARPEGE) and IPSL-CM5a model (LMDz) for April and July

5 Summary and conclusions

The purpose of this study was to better understand the complex behavior of climate models and assess the importance of atmospheric internal dynamics in defining the ITCZ structure. We have investigated the response of two atmospheric general circulation models (ARPEGE-climate and LMDz) in an aquaplanet configuration, to a range of SST latitudinal distributions. We have shown the existence of different regimes of circulation depending on the imposed SST distribution. For large SST gradients in the tropics, a single ITCZ regime is obtained, characterized by one maximum of precipitation confined in the equatorial band. For less important near-equatorial gradients, a double ITCZ structure is simulated with two off-equatorial precipitation peaks. Both of these regimes were found in the two AGCMs. For weaker SST gradients, three precipitation maxima appeared in ARPEGE simulations, whereas this regime was not simulated by the LMDz. The regimes simulated by AGCMs, as well as regime transitions are clearly model-depedendent, with an important role played by the parameterization of moist convection.

We further investigated the mechanisms and feedbacks that drive the transition from the double to the single regime and control the transition threshold. In both models, regime transition is driven by the convergence of the winds at low levels. The atmospheric boundary layer (ABL) flow is driven by the geopotential gradients imprinted on the ABL by the ABLT, that tends to follow the SST through turbulent fluxes. In the LMDz, the low-level convergence is weakened by moist thermodynamics which acts as a negative feedback on ABL geopotential gradients. Two moist feedbacks are identified: on one hand, the dominant effect of the stratospheric cold top on the free-tropospheric convective heating reduces the ABL geopotential gradients; on the other hand, convective downdrafts reduce the ABLT gradients that also decrease the ABL geopotential gradients. In ARPEGE, moist processes have little influence on the ABLT. Horizontal advection feeds back positively on the changes in ABLT so that off-equatorial ABLT gradients are larger than SST gradients.

In summary, the $1P \leftrightarrow 2P$ transition in ARPEGE is modulated by dynamical and dry processes that are mainly controlled by the temperature gradient changes. In the LMDz, regime transition is modulated by a moist thermodynamical control of ABL geopotential gradients; it results in a smoother regime transition compared to that in ARPEGE.

Our work sheds some light on the inner working of the dynamics-thermodynamics interaction in two AGCMs. Following previous studies, we emphasized the role of the low-level humidity convergence in the control of the location of the ITCZ. However, unlike in Charney (1971)'s hypotheses, the SST influences the ITCZ location through its forcing of low-level dynamics (via the ABL temperature gradients created by the surface sensible heat flux) rather than by forcing local convection via the surface flux of moist static energy. This flux appears to be controlled by the low-level wind rather than the SST, and although not negligible, it appears to have a minor influence on the location of the ITCZ compared to the humidity convergence. Also, in both models considered here, the transients have very little influence on the position of the ITCZ organizing convection, in contrast with previous studies that advocated wave-CISK mechanisms (Holton et al. 1971; Lindzen 1974; Hess et al. 1993).

The difference in ITCZ behavior between the two models considered here suggests that there are still very significant differences between state-of-the-art AGCMs in the mechanisms of the interaction between dynamics and convection in the tropics. Since the model propensity to produce a double ITCZ, as well as other systematic biases, results from these mechanisms, it is important to better understand them in order to mitigate precipitation biases in the tropics. In particular, one important finding of this work is the crucial role played by the vertical heating profile in influencing considerably the ABL dynamics. Two important aspects are emphasized: the role of the cold top as a negative feedback on the off-equatorial geopotential gradients throughout the troposphere all the way down to the ABL; and the role of the downdrafts as a negative feedback on the ABLT gradients.

These conclusions are based on simulations in an aquaplanet framework with prescribed SSTs. In order to mitigate the double ITCZ bias in the AGCMs, it is necessary to modify the model design or parameters; this will be addressed in future work. Based on the main conclusion of the present work, the sensitivity of tropical precipitation to some parameters of the convection parameterization will be investigated. In particular, the vertical heating profile associated with convection will be modified by changing the lateral entrainment in convective plumes and downdrafts parameters. A hierarchy of models (coupled ocean-atmosphere model, atmospheric general circulation model and aquaplanet model) might yield a better understanding of the atmospheric dynamics and feedbacks controlling the ITCZ location.

Acknowledgments The authors would like to thank Aurore Voldoire, Sophie Tytecas and Antoinette Alias for their help on the CNRM-CM5 model. We also would like to thank Florent Brient, Laurent Fairhead and Musat Ionela for their help on the IPSL-CM5A model. Thanks are extended to Sandrine Bony, Laurent Li, Hervé Douville, Jean-Luc Redelsperger for helpful discussions throughout the course of this work. Thanks are also due to the editor and reviewers for their helpful comments.

References

Back LE, Bretherthon CS (2008) On the relationship between SST gradients, boundary layer winds and convergence over the tropical oceans. J Clim 22:4182–4196

Barsugli J, Shin SI, Sardeshmukh PD (2005) Tropical climate regimes and global climate sensitivity in a simple setting. J Atmos Sci 62:1226–1240

Belamari S, Pirani A (2007) Validation of the optimal heat and momentum fluxes using the ORCA2-LIM global ocean–ice model. Marine environment and security for the european areaintegrated project (MERSEA IP), deliverable D4.1.3, p 88

Bellon G, Sobel AH (2010) Multiple equilibria of the Hadley circulation in an intermediate–complexity axisymmetric model. J Clim 23:1760–1778

Bjerknes J (1969) Atmospheric teleconnections from the equatorial Pacific. Mon Weather Rev 97:163–172

Bony S, Emanuel JL (2001) A parameterization of the cloudiness associated with cumulus convection; evaluation using TOGA COARE data. J Atmos Sci 58:3158–3183

Bougeault P (1985) A simple parameterisation of the large scale effects of cumulus convection. Mon Weather Rev 4:469–485

Chao WC, Chen B (2004) Single and double ITCZ in an aqua-planet model with constant sea surface temperature and solar angle. Clim Dyn 22:447–459

Charney JG (1971) Tropical cyclogenesis and the formation of the ITCZ. In: Reid WH (ed) Mathematical problems of geophysical fluid dynamics, vol 13, American Mathematical Society, USA, pp 355–368

Cuxart J, Bougeault P, Redelsperger J (2000) A turbulence scheme allowing for mesoscale and large-Eddy simulations. Q J R Meteorol Soc 126:1–30

Dai AG (2006) Precipitation characteristics in 18 coupled climate models. J Clim 19:4605–4630

Déqué M, Dreveton C, Braun A, Cariolle D (1994) The ARPEGE/IFS atmosphere model: a contribution to the French community climate modelling. Clim Dyn 10:249–266

Dijkstra HA, Neelin JD (1995) Ocean–atmosphere interaction and the tropical climatology. Part II: why the Pacific cold tongue is in the east? J Clim 8:1343–1359

Dufresne JL et al. Climate change projections using the IPSL-CM5 earth system model: from CMIP3 to CMIP5. Clim Dyn (submitted)

Emanuel KA (1991) A scheme for representing cumulus convection in large-scale models. J Atmos Sci 48:2313–2335

Fouquart Y, Bonnel B (1980) Computations of solar heating of the earths atmosphere: a new parametrization. Contrib Atmos Phys 53:35–62

Gill AE (1980) Some simple solutions for heat-induced tropical circulation. Q J R Meteorol Soc 106:447–462

Hess PG, Battisti DS, Rasch PJ (1993) Maintenance of the intertropical convergence zones and the tropical circulation on a water-covered earth. J Atmos Sci 50:691–713

Holton JR, Wallace JM, Young JA (1971) On boundary layer dynamics and the ITCZ. J Atmos Sci 28:275–280

Holloway CE, Neelin JD (2007) The convective cold top and quasi equilibrium. J Atmos Sci 64:1467–1487

Hourdin F et al (2006) The LMDZ4 general circulation model: Climate performance and sensitivity to parametrized physics with emphasis on tropical convection. Clim Dyn 27:787–813

Hubert LF, Krueger AF, Winston JS (1969) The double intertropical convergence zone-fact or fiction. J Atmos Sci 26:771–773

Kirtman BP, Schneider EK (2000) A spontaneously generated tropical atmospheric general circulation. J Atmos Sci 57:2080–2093

Lin JL (2007) The double-ITCZ problem in IPCC AR4 coupled GCMs: ocean atmosphere feedback analysis. J Clim 18:4497–4525

Lindzen RS (1974) Wave-CISK in the tropics. J Atmos Sci 31:156–179

Lindzen RS, Nigam S (1987) On the role of the sea surface temperature gradients in forcing the low-level winds and convergence in the tropics. J Atmos Sci 44:2418–2436

Liu Y, Guo L, Wu G, Wang Z (2009) Sensitivity of the ITCZ configuration to cumulus convective parametrizations on an aquaplanet. Clim Dyn 34:223–240

Louis JF (1979) A parametric model of vertical eddy fluxes in the atmosphere. Boundary Layer Meteorol 17:187–202

Mechoso CR and Coauthors (1995) The seasonal cycle over the tropical Pacific in coupled oceanatmosphere general circulation models. Mon Weather Rev 123:2825–2838

Mlawer EJ, Taubman SJ, Brown PD, Iacono MJ, Clough SA (1997) Radiative transfer for inhomogeneous atmospheres: RRTM, a validated correlated-*k* model for the longwave. J Geophys Res 102:16663–16682

Morcrette JJ, Smith L, Fouquart Y (1986) Pressure and temperature dependence of the absorption in longwave radiation parametrizations. Contrib Atmos Phys 59(4):455–469

Neale RB, Hoskins BJ (2000a) A standard test for AGCMs including their physical parameterizations: I: the proposal. Atmos Sci Lett 1:101–107

Neale RB, Hoskins BJ (2000b) A standard test for AGCMs including their physical parameterizations—II: results for the met office model. Atmos Sci Lett 1:108–114

Numaguti A (1993) Dynamics and energy balance of the Hadley circulation and the tropical precipitation zones: significance of the distribution of evaporation. J Atmos Sci 50:1874–1887

Philander SGH, Gu D, Halpern D, Lambert G, Lau NC, Li T, Pacanowski RC (1996) Why the ITCZ is mostly north of the equator? J Clim 9:2958–2972

Ricard JL, Royer JF (1993) A statistical cloud scheme for use in an AGCM. Ann Geophys 11:1095–1115

Schneider EK (2002) Understanding differences between the equatorial Pacific as simulated by two coupled GCMs. J Clim 15:449–469

Voldoire A et al (2011) The CNRM-CM5.1 global climate model: description and basic evaluation. Clim Dyn (in press)

Waliser DE, Somerville RCJ (1994) The preferred latitudes of the intertropical convergence zone. J Atmos Sci 51:1619–1639

Xie SP, Philander SGH (1994) A coupled ocean-atmosphere model of relevance to the ITCZ in the eastern Pacific. Tellus 46A:340–350

Zhang XH, Lin WY, Zhang MH (2007) Toward understanding the double intertropical convergence zone pathology in coupled oceanatmosphere general circulation models. J Geophys Res 112:D12102. doi:10.1029/2006JD007878